Title

Age Associated Increase in Microglia Inflammation and Phagocytosis in the Adult Neural Stem Cell Niche

Authors

Ronald Cutler[1, =], Samuel Harrison[1, =], Natalia Sandoval-Kuhn[1], Stephen Tomlinson[2], Erzsebet Kokovay[1, *]

Affiliations

[1] UTH-SA, Department of Cell Systems and Anatomy, San Antonio, TX, USA 78229

[2] Medical University of South Carolina, Department of Pharmacology and Immunology, Charleston, SC, USA 29425

[=] Authors contributed equally to this work

[*] Correspondence to E.K. (KokovayE@uthscsa.edu)

Number of pages = 38

Number of figures: Main = 4, Supplementary = 5

Number of tables: Main = 0, Supplementary = 6

Number of words: Abstract = 137, Introduction = 569, Discussion = 1,272

Conflicts of interest: The authors declare no competing financial interests.

Acknowledgements: This work was supported by funding from the NIH under grants R01NS102448 and T32 AG0201890

Author contributions: E.K. and R.C. designed the research; R.C., S.H., and N.S.K performed the research; S.T. contributed unpublished reagents/analytic tools; R.C. and S.H. analyzed data; R.C. and E.K. wrote the paper.

Abstract

Adult SVZ neurogenesis declines with age, but the niche mechanisms remain incompletely defined. Here, we show that SVZ microglia acquire activation-associated morphology with aging in male and female C57BL/6 mice. Reanalysis of published SVZ single-cell RNA-Seq data revealed that aged microglia upregulate inflammatory and lysosome/phagosome-related gene programs, including multiple phagocytosis-associated receptors and effectors. Functionally, young SVZ-derived microglia exhibit reduced basal phagocytic activity compared with non-SVZ microglia *in vitro*, whereas aged SVZ microglia show increased phagocytosis. *In vivo* SVZ wholemounts reveal increased progenitor-derived material within lysosomal compartments of microglia with age, without an accompanying increase in apoptosis. Inhibiting complement C3 activation partially restores SVZ proliferation in aged mice and coincides with a reduction of progenitor-derived material within lysosomal compartments of aged microglia. These data support a model in which microglial inflammatory signaling and engagement with neural progenitors contributes to age-related suppression of SVZ proliferation.

Significance Statement

Adult neural stem cells support plasticity and may aid repair after brain injury, but this capacity declines with age. We show that microglia in the aging subventricular zone acquire inflammatory and phagocytic programs, increase their lysosomal association with progenitor-derived material, and are linked to reduced progenitor proliferation. Complement inhibition partially restores proliferative output in aged mice, connecting inflammatory signaling to this niche defect. These findings identify age-dependent microglia–progenitor interactions as a mechanism that may limit neural stem cell activity in the adult brain and suggest immune pathways as possible targets for preserving or restoring neurogenic potential during aging.

Introduction

Adult neural stem cells (NSCs) reside in two principal neurogenic niches of the rodent brain: the subgranular zone (SGZ) of the dentate gyrus and the subventricular zone (SVZ) lining the lateral ventricles. In the current study, we are focused on the NSCs in the SVZ niche, which exist in quiescent (qNSCs) and activated (aNSCs) states and generate transit amplifying cells (TACs), that expand and then produce migratory neuroblasts (Alvarez-Buylla & García-Verdugo, 2002; Doetsch et al., 1999; Lim & Alvarez-Buylla, 2016). These neuroblasts migrate from the SVZ through the RMS into the OB where they differentiate and integrate into local circuitry (Alvarez-Buylla & García-Verdugo, 2002). With aging, multiple studies report reduced SVZ neurogenesis accompanied by decreased NSC proliferation, increased NSC quiescence, and diminished NSC pool size (Ahlenius et al., 2025; Cutler & Kokovay, 2020; Enwere et al., 2004; Kalamakis et al., 2019; Maslov et al., 2004; Solano et al., 2016). These findings motivate work aimed at identifying niche-derived mechanisms that constrain activation and lineage progression in the aged SVZ.

Microglia are brain-resident macrophage-lineage cells that survey the parenchyma and shape neural homeostasis through debris clearance, phagocytosis, synapse remodeling, and secretion of signaling factors (Deczkowska et al., 2018). Fate-mapping indicates that microglia originate from early embryonic yolk sac–derived myeloid progenitors that seed the central nervous system and largely self-maintain thereafter (Ginhoux et al., 2010). Microglia constitute a substantial fraction of brain cells (commonly estimated at ~5–15% depending on region and quantification) and display pronounced context-dependent states across development, aging, and disease (Deczkowska et al., 2018).

Several studies suggest that microglia within the SVZ are not interchangeable with microglia in non-neurogenic parenchyma. SVZ-associated microglia exhibit distinct morphological and antigenic features and have been implicated in regulating neurogenesis and progenitor dynamics (Goings et al., 2006; Marshall et al., 2014; Shigemoto-Mogami et al., 2014; Solano et al., 2016; Xavier et al., 2015). Aging is accompanied by microglial state changes in the SVZ, including increased inflammatory and lysosomal programs that precedes the decline of NSC proliferation, raising the possibility that altered microglia–NSC interactions contribute to reduced neurogenesis in the aged SVZ (Solano et al., 2016). Intriguingly, these age-related shifts in microglia towards an activated state are reminiscent of their phenotype in the developing cerebral cortex and SVZ where they have been shown to phagocytose neural precursor cells (Cunningham et al., 2013; Morrison et al., 2023). Furthermore, in a model of cortical ischemic stroke, microglia were reported to phagocytose dying neuroblasts, constraining the endogenous neurogenic response after injury (Nath et al., 2024). Despite evidence that niche inflammation can constrain activation and lineage output, it remains unclear whether aging-associated microglial activation in the SVZ is coupled to changes in microglial phagocytic behavior toward specific NSC populations, and whether inflammatory signaling and phagocytic engagement represent linked or separable mechanisms.

In this study, we test the hypothesis that aging alters SVZ microglial state and microglia–NSC interactions in ways that contribute to diminished progenitor proliferation. We found that during aging, SVZ microglia are characterized by increases in a lysosomal marker and enlarged morphologies, alongside upregulation of pro-inflammatory and phagocytic gene expression signatures, consistent with a pro-phagocytic phenotype. Aged SVZ microglia show increased phagocytosis *in vitro* and *in vivo*, where we found evidence for the engulfment of aNSCs/TACs.

112 Finally, inhibition of complement C3 activation partially restored proliferative measures and
113 reduced aNSC/TAC engulfment, suggesting that microglial inflammatory signaling and progenitor
114 phagocytosis contributes to reduced NSC proliferation during aging.

115

116

117

118

119

120

121

122

123

124

125

126

127

128 # Materials and Methods

129 ## Animals and Interventions

130 Male and female C57BL/6 mice were used in this study either bred at the UTHSA vivarium or
131 acquired from the National Institute of Aging. Young mice (3 months) and aged mice (12 months)
132 were housed in accordance with the University of Texas Health San Antonio Institutional Animal
133 Care and Use Committee and performed in accordance with institutional and federal guidelines
134 and allowed free access to water and standard rodent chow ad libitum.

135 Both male and female C57BL/6 mice received CR2-crry (10µg/1g mouse; Stephen Tomlinson
136 Lab, Medical University of South Carolina) with saline controls via intraperitoneal injection. CR2-
137 crry or saline was administered every other day for a total of 3 doses.

138

139 ## Immunohistochemistry

140 The SVZ was isolated for wholemount (WM) tissue analysis; mice were anesthetized with
141 isoflurane, a cervical dislocation was performed, followed by brain extraction. Brains were placed
142 into cold HIB where they were halved and the septum and hippocampus were removed, and the
143 SVZ was microdissected from the surrounding brain tissue. The SVZ WM was then fixed in fresh
144 4% paraformaldehyde (PFA) for 30 minutes. SVZ WMs were permeabilized in 2% PBST and
145 blocked overnight at 4˚ C in 10% normal donkey serum (NDS). The SVZ WMs were then
146 incubated at 4°C for 4 days with primary antibody in blocking solution, followed by overnight
147 incubation at 4°C with secondary antibody made in blocking solution, and a 5-minute incubation
148 at room temperature (RT) with DAPI (1:1000; Invitrogen, Cat. No. D1306) then mounted on a

149 slide in ProLong Gold antifade reagent (Invitrogen, Cat. No. P36930). Primary antibodies that
150 were used include Iba1 (1:200; Wako, Cat. No. 019-19741 and 1:200; Novus, Cat. No. NB100-
151 1028), CD68 (1:250; BioRad, Cat. No. MCA1957), and Mash1 (1:5000; CosmoBioUSA, Cat. No.
152 SK-T01-003) Cleaved caspase 3 (1:200 Cell Signaling Cat. No D175 5A1E). Species-specific
153 secondary antibodies (Jackson ImmunoResearch) were used at a concentration of 1:500 in SVZ
154 WMs.

155

156 **Immunohistochemistry Quantification**

157 EdU was quantified in the SVZ by making a "Z Project" 2-dimensional image of the Z-stack in
158 ImageJ on 10 random fields of view and hand counting the number of EdU+ nuclei. The number
159 of microglia were quantified by hand counting Iba1+ cells, excluding cells whose cell body
160 touched the image boundary on Zen Microscopy Software (Zeiss). Total CD68 area was quantified
161 by making a "Z project" 2-dimensional image of the Z-stack, using the "Threshold" function, and
162 then the "Analyze particle" function to give total area in µm2 that was then averaged by total
163 number of microglia in each image. Total number of Iba1+ microglia were quantified similarly to
164 EdU+ cells described above. Mash1 colocalization within Iba1+ microglia were quantified by hand
165 counting in Zen Microscopy Software (Zeiss) by examining each Iba1+ microglia's lysosome
166 (CD68+) to determine if each Iba1+CD68+ microglia contained Mash1 colocalization. The
167 number of Mash1+CD68+Iba1+ microglia were then averaged to total number of Iba1+ microglia
168 in each image. There were no microglia that contained Mash1 that were not CD68+. SVZ WMs
169 were analyzed from 15µm thick Z-stacks (15 Z-stacks per WM). Confocal images were obtained
170 with a Zeiss LSM 710 confocal microscope at 40x objective.

171

172 **Single-cell RNA-sequencing quality control and filtering**

173 Quality control of downloaded single-cell RNA-Seq data (see Data Availability) was first
174 performed, which filtered cells where the number of genes or UMIs detected were greater or less
175 than 5 median absolute deviations (MADs) or percent mitochondria reads greater or less than 3
176 MADs, relative to all cells in the dataset. Genes were filtered if detected in less than 10 cells out
177 of all cells in the dataset. Cell identity labels were those assigned by the original analysis.

178

179 **Single-cell RNA-sequencing differential expression and gene set enrichment**
180 **analysis**

181 Pseudobulk samples were created by summing counts of each identified cell type for each
182 biological replicate. The DESeq2 package (Love et al., 2014) was then used to perform differential
183 expression analysis to compare old vs. young groups. Following this the ClusterProfiler package
184 (Yu et al., 2012) was then used to perform gene set enrichment analysis using the gene ontology
185 biological process database or custom annotations.

186

187 **Microglia phagocytosis gene set analysis**

188 Genes associated with known phagocytosis receptors and/or pathways active in microglia were
189 manually curated by searching the Molecular Signatures Database (MsigDB) and the literature
190 (i.e. Complement, Toll-like receptor, TAM receptor, Trem2 receptor, FC gamma, Pr2y6 receptor,

191 Scavenger receptor, Mannose receptor, LRP1 receptor, Galectin-3 adaptor protein, Microglia
192 Activation, Microglia Proliferation, Disease-Associated Microglia (DAM), and Microglia
193 Development). In addition, gene sets related to screens of phagocytosis regulators was obtained
194 from the literature (see Data Availability). These gene sets were then overlapped with the genes
195 that were found to be significantly differentially expressed (adjusted p-value < 0.05) in the
196 microglia old vs. young comparison.

197

198 **Neural stem cell gene set analysis**

199 Genes associated with pathways known to be expressed in cells that are targeted for phagocytosis
200 were manually curated by searching the Molecular Signatures Database (MsigDB) and the
201 literature (i.e. Apoptosis, Opsonization, Antigen Processing and Presentation, "eat-me," "find-
202 me," and "don't eat me"). Because of the lack of genes which were significantly differentially
203 expressed in neural stem cells (i.e. Astrocytes/qNSCs, aNSCs/NPCs and Neuroblasts) in the old
204 vs. young comparison, the ClusterProfiler package was then used to perform gene set enrichment
205 analysis using the manually curated gene sets. The Log_2 fold change of genes within the gene sets
206 found to be significantly enriched in age-related genes expression of neural stem cells.

207

208 **Microglia Isolation and Cell Culture**

209 SVZ microglia were derived by mixed-glial expansion whereas whole brain microglia were
210 MACS-isolated. C57BL/6 mice were injected intraperitoneally with pentobarbital (25µL/mouse)
211 then perfused with cold 1x PBS. SVZ WMs or the remainder of the whole brain excluding the

212 SVZ and cerebellum, hereby referred to as whole brain (WB), were isolated following perfusion.
213 The tissues were minced and dissociated in 50U papain in DMEM/F12 at 37°C for 45 minutes and
214 manually triturated and spun 3x in DMEM. SVZ and WB homogenate were gently pressed through
215 a 70µm cell strainer to remove debris. For mixed glial culture, SVZ homogenate were then plated
216 in a T25 flask coated with poly-L-ornithine (PLO) in neural growth media (DMEM/F12, 5% fetal
217 bovine serum, 1x N2, 10ng/mL EGF, and 10ng/mL bFGF) until a confluent cell monolayer formed.
218 The culture was then fed microglia proliferation media (DMEM/F12, 10% fetal bovine serum, 1x
219 N2, and 20 ng/mL GM-CSF) until microglia could be seen atop the monolayer. Once microglia
220 were present, they were shaken off from the cell monolayer and the SVZ microglia could be plated
221 for further experimentation.

222 For microglia isolated by MACS, following the cell strainer step, WB homogenate was
223 resuspended in HIB and centrifugated at 400G with no brake in 22% Percoll (Sigma-aldrich, Cat.
224 No. P4937) solution to remove myelin from the samples. The WB homogenate was then
225 resuspended in 0.5% bovine serum albumin and incubated with 10µL CD11b Microbeads (cat#
226 130-093-636) per 107 cells. The homogenate was then placed in an LS column (MiltenyiBiotec,
227 Cat. No. 130-042-401) in a QuadroMACS™ separator (MiltenyiBiotec, Cat. No. 130-090-976) to
228 allow for MACS sorting of CD11b + microglia following manufacturer protocols
229 (MiltenyiBiotec). WB microglia were plated in a 6-well plate coated with PLO/laminin (10µg/mL;
230 Sigma-aldrich, Cat. No. L2020) at 250k cells/well in microglia expansion media (DMEM/F12,
231 100 µg/mL PenStrep, 5 µg/mL n-acetyl-L-cysteine, 5 µg/mL Insulin, 100 µg/mL apo-transferrin,
232 100 µg/mL sodium selenite, 1 µg/mL heparin sulfate, 10% fetal bovine serum, 1.5 µg/mL
233 cholesterol, 40 ng/mL M-CSF, 20 ng/mL GM-CSF, and 2 ng/mL TGF-β) adapted from [Bohlen et
234 al., 2017].

235

236 **Microglia *in vitro* Phagocytosis Assay**

237 The phagocytosis assay was performed using live cell imaging by Incucyte S3 (Essen BioScience)
238 for WB or SVZ microglia phagocytosis from 3- or 12-month mice. WB microglia were passaged
239 from a 6-well plate with Trypsin (Fisher, Cat. No. 25-200-072) following MACS isolation and
240 SVZ microglia were collected from mixed glial culture and microglia were plated in a 96 well
241 plate coated with PLO/laminin at 20k cells/well in microglia expansion media for 3 days. After 3
242 days, SVZ and WB microglia were moved to serum free media (DMEM/F12, 100 µg/mL PenStrep,
243 5 µg/mL n-acetyl-L-cysteine, 5 µg/mL Insulin, 100 µg/mL apo-transferrin, 100 µg/mL sodium
244 selenite, 1 µg/mL heparin sulfate, 1.5 µg/mL cholesterol, 40 ng/mL M-CSF, and 2 ng/mL TGF-β)
245 adapted from [Bohlen et al., 2017] for 1 week. All microglia were then incubated with 5 µg/mL
246 Isolectin IB4 Alexa Fluor™ 488 Conjugate (Invitrogen, Cat. No. I21411) for 60 minutes at 37°C.
247 SVZ or WB microglia of both ages were treated with Zymosan S. cerevisiae BioParticles™ (10
248 mg/mL; Invitrogen, Cat. No. Z2849) conjugated pHrodo™ Red SE (Molecular Probes™, Cat. No.
249 P36600) following manufacturer protocols (ThermoFisher) and adapted from [Haney et al., 2018;
250 Pluvinage et al., 2019], both Zymosan-pHrodo and Cytochalasin D (10 mM/µL Sigma-aldrich,
251 Cat. No. C8273) to inhibit phagocytosis, or isolectin only as a negative control. The microglia
252 were then incubated in the Incucyte S3 with fluorescent images captured every hour over the
253 course of 48 hours for live cell imaging of microglia phagocytosis. The images were analyzed in
254 the IncuCyte software (Essen BioScience) quantifying colocalization of the green fluorescence of
255 Isolectin IB4 labelled microglia and the red fluorescence of engulfed Zymosan-pHrodo within the
256 microglia lysosome demonstrating microglia phagocytosis. Total pHrodo area / number of

257 microglia was calculated for each well and condition yielding amount of in vitro phagocytosis
258 occurring at each time point.

259

260 RNA Extraction and qPCR

261 RNA was extracted from freshly isolated microglia following magnetic-activated cell sorting
262 (MACS) isolation, using a TRIzol-chloroform method (Rio et al., 2010) where cells were lysed in
263 TRIzol (Invitrogen, Cat. No. 15596018), aqueous layer separated with chloroform, RNA was
264 precipitated with isopropanol, washed in ethanol, dried, then resuspended in RNase-free water.
265 cDNA was synthesized using High Capacity cDNA Reverse Transcription Kit (Applied
266 Biosystems, Cat. No. 4368814). Quantitative polymerase chain reaction (qPCR) was performed
267 using a C1000 Touch Thermal Cycler (BioRad) with iTaq™ Universal SYBR® Green Supermix
268 (BioRad, Cat. No. 1725121). Reactions were performed in doublet with glyceraldehyde-3-
269 phosphate dehydrogenase (GAPDH) used as an endogenous control. Negative control reactions
270 were performed using the same conditions without cDNA. Quantification was analyzed using the
271 ΔΔCt method as described [(Livak & Schmittgen, 2001)]. Primers were used for the following
272 transcripts: C1QA, P2Y12, TREM2, LPAR, C3, CR1, ITGAM, ITGAX, GAPDH.

Primers	Forward	Reverse
C1QA	AAAGGCAATCCAGGCAATATCA	TGGTTCTGGTATGGACTCTCC
C3	CCAGCTCCCCATTAGCTCTG	GCACTTGCCTCTTTAGGAAGTC
TREM2	CTGGAACCGTCACCATCACTC	CGAAACTCGATGACTCCTCGG
LPAR	AGCCATGAACGAACAACAGTG	CATGATGAACACGCAAACAGTG

CR1	ATGGAGGTCTCTTCTCGGAGT	GGCCGAAGGCTACAAGGAG
ITGAM	GGGAGGACAAAAACTGCCTCA	ACAACTAGGATCTTCGCAGCAT
ITGAX	CTGGATAGCCTTTCTTCTGCTG	GCACACTGTGTCCGAACTCA
GAPDH	AGGTCGGTGTGAACGGATTTG	TGTAGACCATGTAGTTGAGGTCA

EdU Labeling and Staining

Mice were injected intraperitoneally (50µg EdU/1g mouse) 2 hours before sacrifice. Their brains were removed and SVZ was isolated and fixed for 30 minutes in 4% PFA. EdU staining was performed following manufacturer protocols (Fisher, Click-it EdU Imaging Kit, Cat. No. C10337).

Experimental Design and Statistical Analysis

Student's t-tests and two-way ANOVA were used to analyze the data on GraphPad Prism 8 Software. All data are expressed as mean ± standard error of the mean.

Data Accessibility

Normalized single-cell RNA-sequencing data and cell type annotations of the SVZ from young (3 months old) and old (28–29 months old) male mice (n = 3) was downloaded from Supplementary Table 2 of the Dulken et al., 2019 study. Results of screen for phagocytosis regulator genes were downloaded from Supplementary Table 5 of the Haney et al., 2019 study and Supplementary Table 2 of the Pluvinage et al., 2019 study. Marker genes of major cell types in the SVZ of young (2-4

289 months old) male and female mice were downloaded from Table S1 of the Zywitza et al., 2018
290 study.
291

292 Code Accessibility

293 Code to reproduce single-cell RNA-sequencing data analyses is available at the following
294 repository: https://github.com/cutleraging/nsc-aging
295
296
297
298
299
300
301
302
303
304
305
306

307 # Results

308 ## Age-related changes in SVZ microglia morphology

309 We have previously reported that murine SVZ neurogenesis is reduced by 12 months of age
310 (Solano et al., 2016). To assess how SVZ microglia change during aging, we performed
311 immunohistochemistry on SVZ wholemount preparations (to preserve 3D niche cytoarchitecture)
312 from young (3 month) and aged (12 month) mice, staining for the microglial marker Iba1 and the
313 lysosomal marker CD68. In young mice, Iba1+ microglia exhibited a ramified morphology
314 throughout the SVZ with relatively low CD68 signal within Iba1+ cells (Fig. 1A-B). In aged mice,
315 Iba1+ microglia displayed morphology consistent with activation, including fewer processes and
316 enlarged somata, together with increased CD68 signal within Iba1+ cells (Fig. 1C-D). Because
317 microglia can adopt a lysosome-rich, phagocytic phenotype during neuronal development that is
318 associated with engulfment of neural precursor cells, we hypothesized that age-associated
319 microglial activation in the SVZ is accompanied by increased phagocytic activity toward SVZ
320 progenitors (Cunningham et al., 2013).

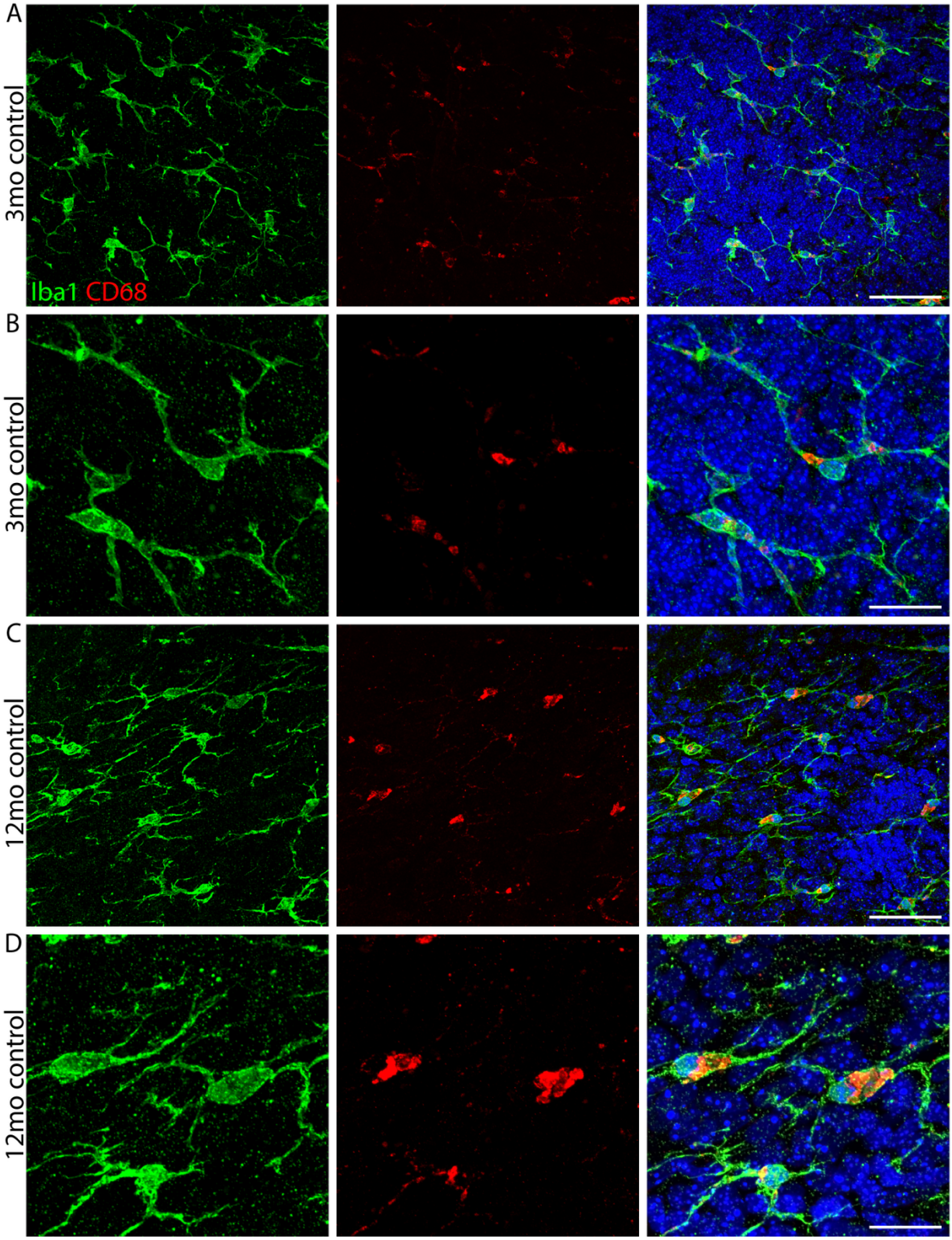
A
3mo control
Iba1 CD68
B
3mo control
C
12mo control
D
12mo control

321

322 **Figure 1. Age-Associated SVZ Microglia Morphological Changes and Increased Activation.**
323 Representative confocal projection images of SVZ microglia stained with Iba1 (green), lysosomes
324 stained with CD68 (red), and nuclei stained with DAPI (blue). **(A-B)** Young (3 month) SVZ
325 microglia imaged at 40X magnification (A) or 100X magnification (B). **(C-D)** Aged (12 month)
326 SVZ microglia imaged at 40X magnification (C) or 100X magnification (D). Scale bars in (A) and
327 (C) = 20µm, scale bars in (B) and (D) = 50µm

328

329 Gene expression in the aging SVZ suggests increased microglial phagocytic 330 programs

331 To assess age-related transcriptional changes in SVZ microglia and NSC populations relevant to
332 inflammation and phagocytosis, we reanalyzed a published single-cell RNA-Seq dataset
333 comprising of 14,685 cells from the SVZ of young (3 month) and old (28/29 month) male mice
334 (Dulken et al., 2019). We generated pseudobulk profiles for each cell type and biological replicate,
335 performed differential gene expression analysis (old vs. young), followed with gene set enrichment
336 analysis (GSEA) (Supplementary Figs. 1A-B).

337 In microglia, we identified 254 genes significantly upregulated and 54 genes significantly
338 downregulated with age (adjusted p-value < 0.05; Supplementary Fig. 1C; Supplementary Table
339 1). GSEA of genes upregulated with aging revealed enrichment of processes related to translation,
340 secretion of inflammatory cytokines, and lipid metabolism, consistent with prior analyses (Dulken
341 et al., 2019; Yen & Yu, 2024). In contrast, downregulated genes were enriched for cytoskeleton
342 organization terms, which has not been previously reported and may suggest dysfunction in
343 motility or morphology-related programs (Supplementary Fig. 1D).

344 Although canonical "phagocytosis" terms were not significantly enriched by GSEA
345 (Supplementary Fig. 1D), several phagocytosis-associated receptors, including *Axl* and *Tlr2*, were
346 among the most strongly upregulated transcripts with age (Supplementary Fig. 1C). We therefore
347 curated comprehensive gene sets representing multiple components of phagocytosis from MSigDB
348 (Liberzon et al., 2024) and intersected these with age-related differentially expressed genes
349 (ARDEGs; adjusted p-value < 0.05; Supplementary Table 2). 19 phagocytosis-related genes
350 overlapped with the microglia ARDEG set, of which 18 were upregulated in aged microglia (Fig.
351 2A; Supplementary Table 3). Notably, 8 of these genes (*Cyba, Atp6v0e, Rab7b, Cybb, Vim, B2m,*
352 *Tlr2,* and *Hvcn1*) are linked to phagosome formation/maturation and vesicular acidification. We
353 further expanded our phagocytosis gene list to include genes identified in prior functional screens
354 (Haney et al., 2018; Pluvinage et al., 2019), and found that all intersecting genes (9/9) were
355 upregulated in aged microglia (Supplementary Figs. 2A-B). Finally, we found that the broad
356 upregulation of phagocytosis-related gene expression was also accompanied by an increase in the
357 expression of genes related to microglia activation (Supplementary Figs. 2C-D). While these
358 transcriptional shifts are consistent with increased lysosomal/phagocytic programs, we note that
359 elevated expression of such genes could also reflect compensatory responses to altered phagocytic
360 demand or efficiency rather than a direct readout of increased engulfment per se. For instance, the
361 expression of the receptor essential for microglial function, *Csf1r*, was downregulated in aged
362 microglia while the ligand *Csf1* showed the opposite trend and thus may be a compensatory
363 response to chronic microglia activation (Supplementary Fig. 2C) (Hu et al., 2024). Together, these
364 findings suggest that aging is accompanied by transcriptional reprogramming of SVZ microglia
365 toward states featuring inflammatory signaling and lysosome/phagosome-related programs, with

366 partial resemblance to developmental and phagocytic microglial states (Cunningham et al., 2013;
367 Izgi et al., 2022).

368 We next asked whether age-associated changes were concentrated within particular receptor-
369 mediated phagocytosis pathways. Using a curated list for the major phagocytosis pathways, we
370 observed upregulation of the receptors in the Complement, TAM, and Toll-like pathways (Fig. 2B;
371 Supplementary Table 3). In contrast, for the FC gamma, Scavenger, P2ry6, and Trem2 receptor
372 pathways, multiple pathway components were consistently upregulated without a corresponding
373 increase in the core receptor transcript (Deczkowska et al., 2018). Notably, while Trem2 itself was
374 not increased, aged microglia displayed expression patterns consistent with a disease-associated
375 microglia (DAM) stage 2 signature that has been reported to be Trem2-dependent in other contexts
376 (Supplementary Fig. 2E). Overall, these results indicate broad multi-pathway upregulation of
377 phagocytosis-related gene expression during aging and suggest that aged SVZ microglia may
378 adopt a unique Trem2-independent DAM-like state.

379 We then analyzed NSC populations for age-associated expression changes in signals relevant to
380 target-cell recognition and engulfment, including apoptosis, "find-me," "eat-me," and "don't eat-
381 me" programs. Compared to microglia, there were very few ARDEGs: 13 genes were significantly
382 upregulated in aged astrocyte-qNSC as compared to young (adjusted p-value < 0.05), whereas no
383 genes met this threshold for aged aNSC, TACs or neuroblasts (Supplementary Figs. 1E-J). Given
384 this limited power for threshold-based overlap analyses, we used GSEA with curated gene sets for
385 apoptosis and phagocytosis-related signaling (Supplementary Table 2).

386 Using this approach, we detected age-associated upregulation of an apoptosis gene set in astrocyte-
387 qNSC cells (adjusted p-value < 0.05), whereas aNSC, TACs and neuroblasts showed the opposite
388 trend (Fig. 2C; Supplementary Fig. 3A). We did not detect significant enrichment for curated "find-

me" or generic "eat-me" gene sets. However, we observed age-associated upregulation of complement system and opsonization gene sets (often considered "eat-me"–adjacent signals) in astrocyte-qNSCs and neuroblasts, but not in aNSCs or TACs (Fig. 2C; Supplementary Fig. 3B,C) (Li, 2012). Intriguingly, astrocyte-qNSCs and neuroblasts also showed increased expression of a curated "don't eat-me" gene set (Fig. 2C; Supplementary Fig. 3D). This set includes genes related to MHC class I antigen presentation such as *H2-K1* and *H2-D1*, which in some contexts can oppose macrophage phagocytosis, particularly when expressed with *B2m* (Supplementary Fig. 3D) (Khalaji et al., 2023). Consistent with a potential receptor–ligand axis, *Lilrb4a*, an inhibitory receptor for MHC class I, was among the age-upregulated microglial ARDEGs (Supplementary Fig. 1C). An antigen processing/presentation gene set showed a similar pattern to the "don't eat-me" set, further supporting increased MHC class I–associated programs in aged astrocyte-qNSCs and neuroblasts, but not aNSC-NPCs (Supplementary Fig. 1E).

In summary, transcriptomic changes in SVZ microglia with age are consistent with increased inflammatory and lysosome/phagosome-related programs across multiple receptor pathways. In aged NSC populations, astrocyte-qNSCs and neuroblasts showed increased complement pathway components ("eat-me" signals) together with increased expression of putative "don't eat-me" anti-phagocytic signals, while aNSC-NPCs did not show comparable upregulation of those signals. These patterns are consistent with a model in which age-associated microglial phagocytic programs may preferentially engage aNSC/TACs.

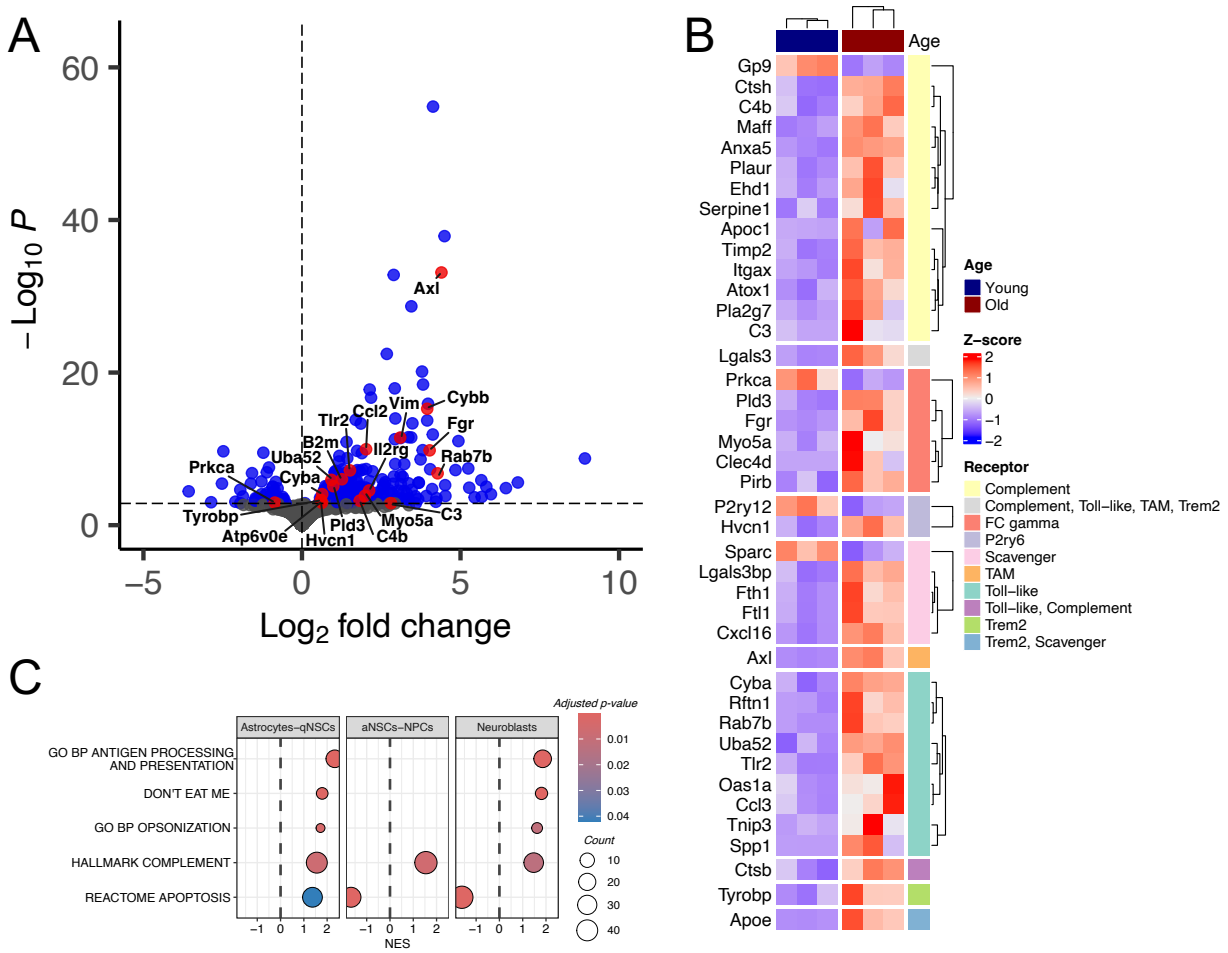

409

410 **Figure 2. Gene expression in the aging SVZ suggests increased microglial phagocytic**
411 **programs**

412 **(A)** Pseudobulk level analysis of differential gene expression changes during aging of young (3
413 month) and aged (28–29 month) microglia in the SVZ. Red points indicate genes that overlapped
414 with the phagocytosis-related gene sets (Supplementary table 2) which have absolute log2 fold
415 change > 1 and adjusted p-value < 0.05. Statistics: n=3 mice/group, DGE results obtained using
416 Wald test followed by Benjamini-Hochberg correction for multiple hypothesis testing. **(B)**
417 Heatmap of age-related DEGs (adjusted p-value < 0.05) in aging SVZ microglia (obtained from
418 analysis in (A)) that overlapped with phagocytosis-related gene sets (Supplementary table 2)

419 Statistics: n=3 mice/group. **(C)** Gene set enrichment analysis of age-related gene expression
420 changes in neural progenitor cells using apoptosis, "find-me," "eat-me," and "don't eat-me" signal
421 gene sets (Supplementary table 2). Statistics: n=3 mice/group, GSEA p-values obtained using a
422 permutation test followed by Benjamini-Hochberg correction for multiple hypothesis testing.

423

424 SVZ microglia show an age-associated increase in phagocytic activity toward 425 SVZ progenitors

426 To assess SVZ microglia phagocytic activity, we microdissected the SVZ and isolated microglia
427 either from the SVZ or from the remainder of the brain (excluding the SVZ) from young (3 month)
428 and aged (12 month) mice. Isolated microglia were expanded *in vitro*, and phagocytosis was
429 quantified by live imaging of engulfment of pHrodo-conjugated yeast particles (pH-sensitive
430 reporter that fluoresces upon acidification in phagolysosomes) (Kapellos et al., 2016). In young
431 animals, SVZ-derived microglia displayed lower phagocytic activity than microglia isolated from
432 non-SVZ brain regions under our assay conditions, consistent with niche-associated specialization
433 toward reduced basal phagocytosis (Fig. 3A) (Xavier et al., 2015). In aged animals, SVZ-derived
434 microglia showed a significant increase in phagocytic activity relative to young SVZ microglia,
435 approaching the levels observed in whole-brain microglia.

436 We next sought *in vivo* evidence that the age-associated increase in SVZ microglial phenotypes
437 reflects increased phagocytic engagement with SVZ progenitors. As an initial test, we quantified
438 apoptosis in the SVZ by immunohistochemistry for cleaved caspase-3 on coronal sections from
439 young (3 month) and aged (12 month) mice and did not detect a significant age-associated increase
440 in apoptotic cells in the SVZ (Fig. 3B). Next, we sought to validate the findings of an age-related

441 increase in SVZ microglia phagocytosis activity in our *in vitro* system by examining SVZ
442 microglia phagocytosis *in vivo*. We assessed microglial phagolysosomal content directly by
443 staining SVZ wholemounts for Iba1 (microglia), CD68 (lysosomes), and Mash1 (aNSC/TAC
444 specific transcription factor) (Kim et al., 2011; Lim & Alvarez-Buylla, 2016). In both young and
445 aged SVZ, we observed Mash1 signal within CD68+ compartments inside Iba1+ microglia (Fig.
446 3D). Quantification indicated that ~20% of SVZ microglia contained Mash1+ material within
447 CD68+ compartments in young mice, and this fraction increased over 2-fold at 12 months of age
448 (Fig. 3C). Together, these in vitro and in vivo data support an age-associated increase in SVZ
449 microglial phagocytic activity and increased microglial phagolysosomal association with
450 progenitor-derived material in the aged SVZ.

451

452

453

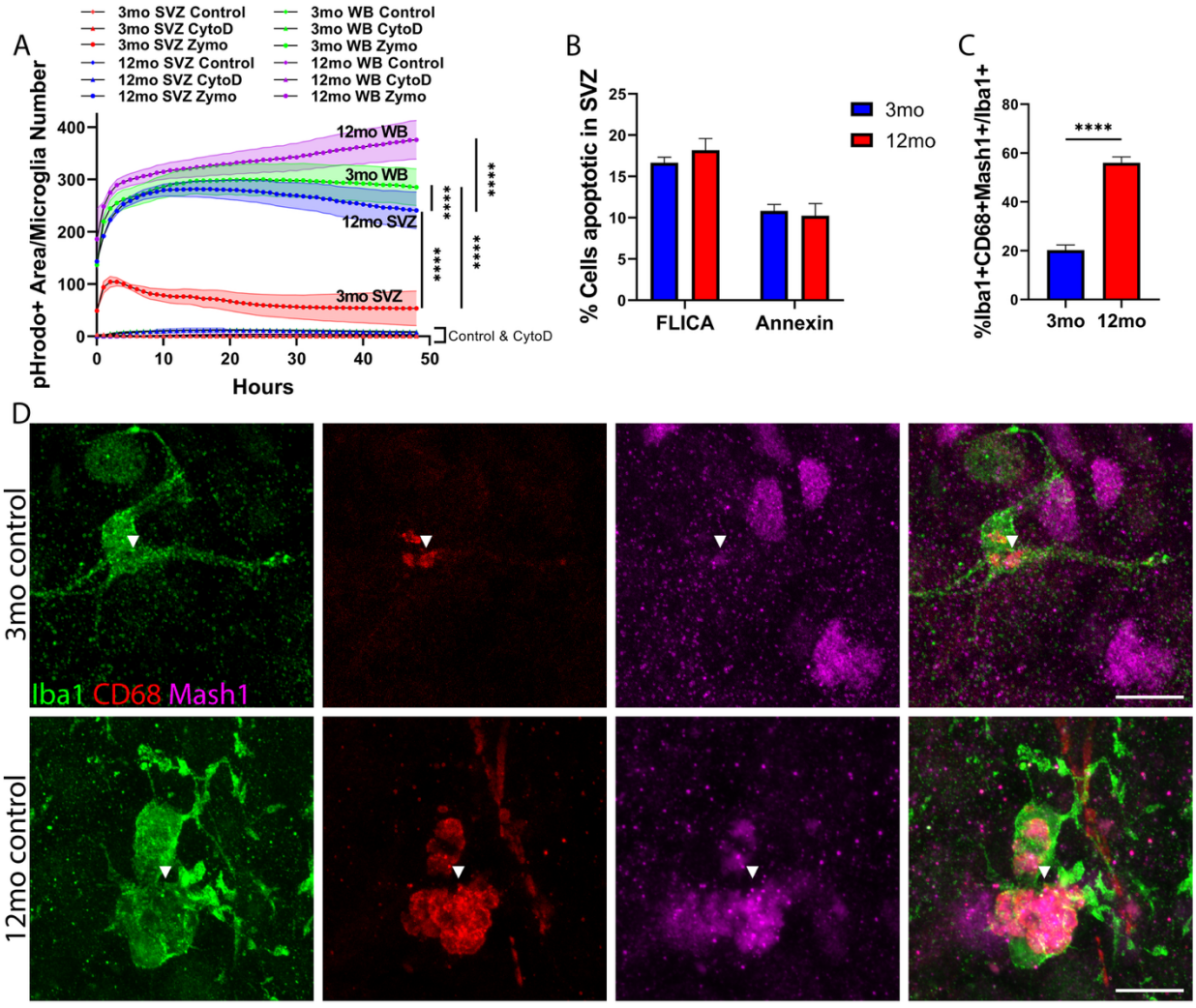

Figure 3. SVZ microglia show an age-associated increase in phagocytic activity toward SVZ progenitors. (A) Time-lapse *in vitro* phagocytosis assay of young (3 months) or aged (12 months) SVZ or whole brain (WB) microglia labeled with isolectin and incubated with Zymosan-pHrodo (Zymo), CytochalasinD and Zymosan-pHrodo (CytoD, negative control), or isolectin only (Control). Phagocytosis is quantified as pHrodo+ area indicated by red fluorescence / microglia number. Statistics: n=3 mice/group, ≥ 1,000 microglia quantified per mouse. (B) Quantification of apoptosis in SVZ whole mounts. Statistics: n=6 mice/group, p-value estimated using two-way ANOVA. (C) Quantification of *in vivo* phagocytosis of 3- or 12-month SVZ microglia measured

463 as Iba1+CD68+Mash1+ microglia / total Iba1+ microglia (Methods). *n*=11 mice/group, ≥100
464 microglia quantified per mouse. (D) Representative confocal projection images of young or aged
465 SVZ microglia stained with Iba1 (green), microglia lysosomes stained with CD68 (red), and TAC
466 transcription factor stained with Mash1 (magenta). Scale bar: 10µm, p-value estimated using two-
467 way ANOVA. P-value legend: ns: no symbol; ****: $p \leq 0.0001$.

468

469 **Complement inhibition partially rescues SVZ proliferation in aged mice**

470 To explore possible mechanisms that might contribute to the age-associated increase in SVZ
471 microglial phagocytic engagement of aNSC/TAC populations in the SVZ, we examined expression
472 of candidate pro-inflammatory factors in SVZ microglia guided by our transcriptomic reanalysis
473 (Fig. 2A). We reasoned that pro-inflammatory genes that were low or absent in the young SVZ
474 microglia relative to non-SVZ microglia that are increased with age in SVZ microglia would be
475 good candidates based on our *in vitro* phagocytosis results (Fig. 3A). Among the candidates, *C3*
476 (Complement component 3) showed higher expression in non-SVZ microglia relative to young
477 SVZ microglia and was strongly upregulated with age in SVZ microglia (Supplementary Fig. 4).
478 In addition, transcripts encoding *C3* receptors *Itgam* and *Itgax* were increased in aged SVZ
479 microglia. Based on these observations, we tested whether inhibiting *C3* activation would alter
480 SVZ proliferation and/or microglial phagocytic readouts *in vivo*.

481 To inhibit C3 cleavage and deposition, we used CR2-Crry, a targeted complement inhibitor that
482 crosses the blood brain barrier and localizes to sites of complement activation via CR2 to then
483 block C3 activation through Crry (Atkinson et al., 2005; Song et al., 2003). Young (3 month) and
484 aged (12 month) mice received CR2-Crry or saline every other day for three total doses, followed

485 by a 2-hour EdU pulse prior to sacrifice to label proliferating cells (Fig. 4A). SVZ wholemounts
486 were collected and processed for immunohistochemistry as described above (Methods).

487 In young mice, CR2-Crry treatment did not significantly affect SVZ proliferation as indicated by
488 EdU+ cells, microglial CD68 area, or the fraction of microglia containing Mash1+ material within
489 CD68+ compartments (Fig. 4C). As expected, saline-treated aged mice showed reduced SVZ
490 proliferation relative to saline-treated young mice (Fig. 4B). In aged mice, CR2-Crry significantly
491 increased SVZ proliferation and Mash1+ cells compared with age-matched saline controls as
492 indicated by EdU+ cells (Fig. 4B; Supplementary Fig. 5). CD68 area per Iba1+ microglia was
493 increased in aged saline-treated mice relative to young controls, while CR2-Crry produced a non-
494 significant reduction in this measure in aged mice (Fig. 4D). Similarly, the microglia containing
495 Mash1+ material within CD68+ compartments increased with age, and CR2-Crry treatment
496 resulted in a non-significant reduction relative to aged saline controls (Fig. 4E). Together, these
497 data indicate that complement inhibition via CR2-Crry can partially restore proliferative output in
498 the aged SVZ.

499

500

501

502

503

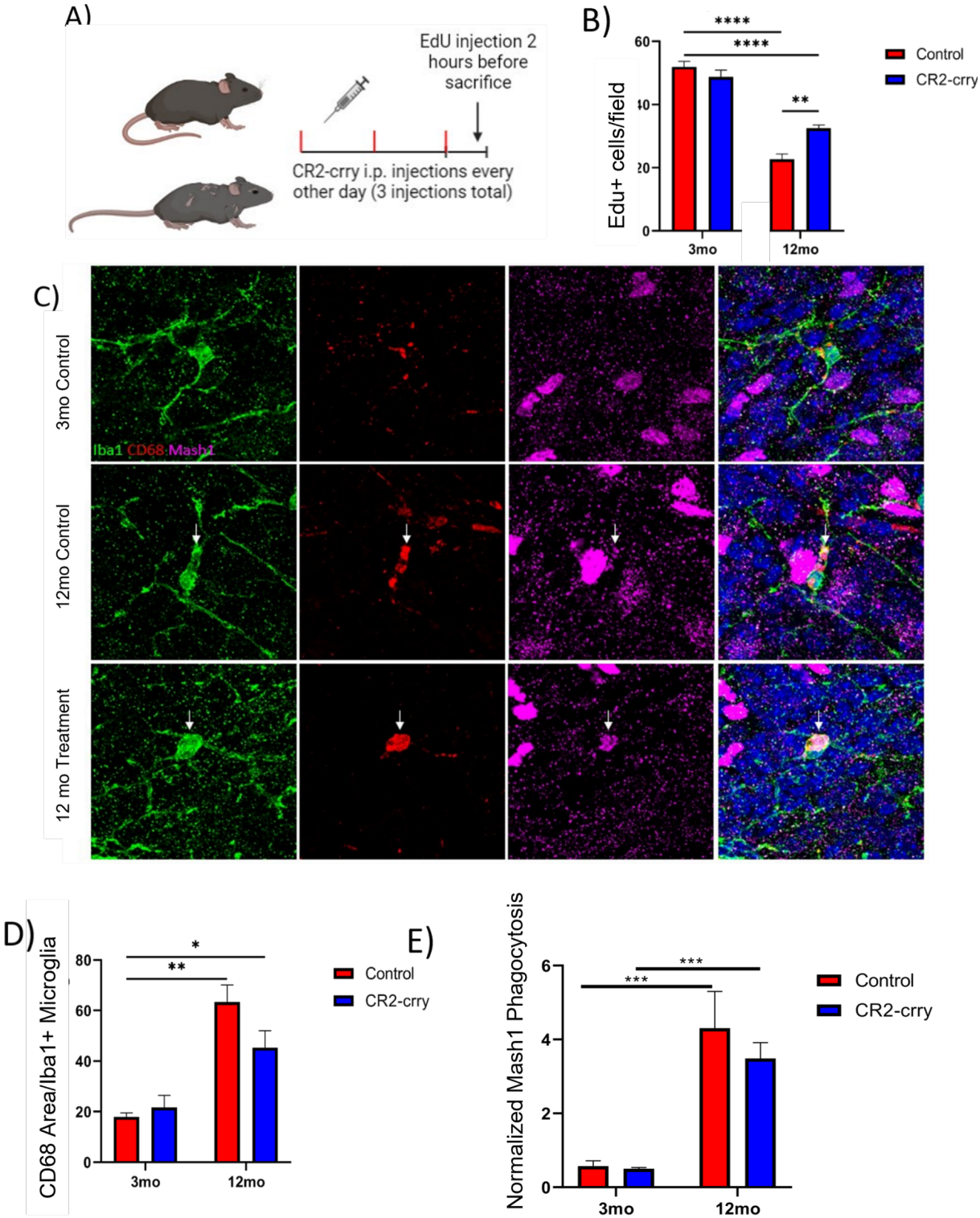
A)
EdU injection 2 hours before sacrifice
CR2-crry i.p. injections every other day (3 injections total)
B)
Edu+ cells/field
Control
CR2-crry
3mo
12mo
C)
3mo Control
12mo Control
12 mo Treatment
Iba1 CD68 Mash1
D)
CD68 Area/Iba1+ Microglia
Control
CR2-crry
3mo
12mo
E)
Normalized Mash1 Phagocytosis
Control
CR2-crry
3mo
12mo

504

505 **Figure 4. Complement inhibition partially rescues SVZ proliferation in aged mice (A)**
506 Graphic representation of CR2-crry or saline administration to young (3 month) or aged (12
507 month) mice. **(B)** Quantification of proliferating EdU-positive cells in the SVZ of young or aged
508 control or CR2-crry treated mice. Statistics: *n*=4 mice/group, ≥ 100 image fields quantified per
509 mouse, p-values estimated using two-way ANOVA. **(C)** Confocal projection images of young
510 control, aged control, aged CR2-crry treated SVZ microglia stained with Iba1 (green), microglia
511 lysosomes stained with CD68 (red), and aNSC/TAC transcription factor stained with Mash1
512 (magenta). Arrowheads in aged control and aged CR2-crry treated indicate colocalization of
513 Mash1+ signal within microglia lysosomes (Iba1+CD68+). Scale bar: 10µm. **(D)** Quantification
514 of microglia activation measured by CD68 area / Iba1+ cells. Statistics: *n*=4 mice/group, ≥ 1,000
515 microglia quantified per mouse, p-values estimated using two-way ANOVA. **(E)** Quantification of
516 Mash1 containing microglia (Iba1+CD68+Mash1+ / Iba1+ cells / Mash1+ cells) from young or
517 aged control or CR2-crry treated mice. Statistics: Same as in (D). P-value legend: ns: no symbol;
518 *: $p \leq 0.05$, **: $p \leq 0.01$, ***: $p \leq 0.001$, ****: $p \leq 0.0001$.

519
520
521
522
523
524
525
526

527 # Discussion

528 Adult SVZ NSCs generate new neurons that migrate to the OB and contribute to olfactory learning
529 and discrimination throughout life (Lledo & Valley, 2016). In addition, following brain injury SVZ
530 neural progenitors and neuroblast undergo a proliferative burst and then migrate to damaged areas
531 where they give rise to a limited number of neurons, astrocytes and oligodendrocytes and can also
532 secrete pro-reparative factors (Liang et al., 2019; Robin et al., 2006; Yamashita et al., 2006). The
533 blockade of this response results in larger lesions and worsens behavioral deficits (Ohab et al.,
534 2006). Together, these observations support the SVZ as a candidate target for therapies aimed at
535 enhancing endogenous repair. However, SVZ neurogenesis declines drastically in aged rodents,
536 with the most-rapid reductions between midlife (9-12 months) and persists for the duration of
537 aging (Luo et al., 2006). This decline coincides with increasing risk of brain injury with age,
538 motivating a need to identify niche mechanisms that constrain SVZ stem/progenitor function. Our
539 data support a model in which aging is accompanied by increased microglial inflammatory and
540 phagocytic programs within the SVZ niche, together contributing to reduced stem/progenitor
541 output during aging.

542 During embryonic neurogenesis, SVZ-associated microglia display amoeboid morphology and can
543 regulate precursor pool size through phagocytosis of non-apoptotic neuroblasts (Cunningham et
544 al., 2013; Morrison et al., 2023). In the adult dentate gyrus, another neurogenic niche, microglia
545 phagocytose apoptotic newborn neurons as part of routine homeostasis, whereas apoptosis within
546 the adult SVZ is generally reported to be low (Luo et al., 2006). In the OB, where many SVZ-
547 derived neurons fail to integrate, phagocytic clearance is more prominent (Xavier et al., 2015). In
548 our study, we did not detect an age-associated increase in apoptotic signal in the SVZ, arguing
549 against a simple model in which increased microglial lysosomal content in aging is driven

550 primarily by increased clearance of apoptotic SVZ progenitors. Instead, our *in vivo* colocalization
551 and *in vitro* phagocytosis assays are consistent with increased microglial phagocytic programs and
552 increased microglial association with Mash1+ progenitor-derived material in the aged niche,
553 although we emphasize that colocalization-based metrics are proxies and do not, on their own,
554 establish engulfment kinetics or target selectivity.

555 Reanalysis of published single-cell transcriptomes from young and old SVZ provided an
556 independent line of evidence consistent with increased inflammatory and phagocytosis-related
557 programs in aged microglia. In pseudobulk AGDGE and gene-set analyses, aged microglia
558 upregulated inflammatory signaling and lysosome/phagosome-associated genes, including
559 multiple receptors and effectors linked to phagocytic function (e.g., *Axl*, *Tlr2*, *Lgal3*, and *C3*), and
560 showed broader increases across several phagocytosis pathway components (e.g. Complement, FC
561 gamma, and Toll-like). In contrast, neural stem/progenitor populations exhibited comparatively
562 few significant age-related DE genes, motivating gene-set–level testing rather than threshold
563 overlaps. Those analyses suggested that astrocyte-qNSCs and neuroblasts increase
564 complement/opsonization-related expression (i.e. "eat-me" programs) while also increasing
565 expression of putative anti-phagocytic programs, including MHC class I/antigen presentation–
566 associated genes (i.e. "don't eat-me" programs). aNSCs-NPCs did not show the same pattern of
567 increased "don't eat-me" programs, which is consistent with, but does not prove, a model in which
568 aNSCs/ TACs may be relatively vulnerable to microglial phagocytic engagement in the aged niche.
569 Importantly, transcriptomic signatures cannot distinguish increased phagocytic capacity from
570 compensatory responses to altered substrate availability, nor can they assign directionality without
571 functional validation. The strength of the scRNA-seq analysis is therefore as mechanistic context
572 that complements the *in vivo* and *in vitro* assays.

573 Microglia are distributed throughout the brain, but exhibit region-dependent heterogeneity in
574 density, morphology, transcriptional state, and receptor expression shaped by local
575 microenvironments (Grabert et al., 2016; Tan et al., 2020). SVZ microglia are reported to be
576 phenotypically distinct from non-germinal regions, supporting the idea of niche specialization
577 (Goings et al., 2006; Marshall et al., 2014; Shigemoto-Mogami et al., 2014; Solano et al., 2016;
578 Xavier et al., 2015). Riberio Xavier et al. showed that SVZ microglia in young adults have distinct
579 morphology and receptor profiles, are required for neuroblast survival and migration, and display
580 comparatively low phagocytic activity in the young SVZ niche, potentially linked to reduced
581 expression of specific purinergic receptors (Xavier et al., 2015). Our *in vitro* assay is consistent
582 with this niche-specific baseline state. SVZ-derived microglia from young mice exhibited lower
583 phagocytic activity than microglia isolated from non-SVZ brain regions. With aging, we observe
584 a shift toward increased CD68+ lysosomal features and increased phagocytic readouts, consistent
585 with remodeling of this niche-specialized state.

586 To probe whether inflammatory signaling contributes causally to SVZ aging phenotypes, we used
587 CR2-Crry, a targeted inhibitor of complement C3 activation and deposition (Atkinson et al., 2005;
588 Song et al., 2003) that crosses the blood brain barrier (Alawieh et al., 2018). This intervention
589 partially rescued SVZ proliferation in aged mice, supporting the conclusion that complement-
590 linked signaling contributes to the age-associated reduction in proliferative output. Although
591 insignificant, CR2-Crry treatment reduced microglia inflammation and Mash1+ material within
592 CD68+ compartments in aged microglia. Future work will be aimed at the direct quantification of
593 engulfment dynamics, and mechanistic tests of candidate receptor–ligand axes suggested by the
594 transcriptomic analyses.

595 Finally, our transcriptomic observations raise a testable hypothesis about target susceptibility.
596 Aging may increase "eat-me" programs in multiple SVZ populations, while "don't eat-me"
597 programs may be relatively stronger in astrocyte-qNSCs and neuroblasts than in aNSCs and TACs.
598 If validated, this could help explain why increased microglial phagocytic programs in aging are
599 associated with progenitor loss while sparing other SVZ populations. Future work should directly
600 test whether differences in cell-surface inhibitory cues (e.g., *Cd200*, *Pecam1*, MHC class I–linked
601 programs) and corresponding microglial inhibitory receptors shape selective engagement of
602 progenitors in the aged niche, and whether manipulating these interactions can decouple restored
603 proliferation from progenitor loss, potentially paving the way for future therapeutics.

604 Several limitations should be considered when interpreting these findings. First, our *in vivo*
605 phagocytosis readout relies on confocal colocalization of Mash1 signal within CD68+
606 compartments in Iba1+ microglia in SVZ wholemounts. While this pattern is consistent with
607 phagolysosomal internalization, additional validation using phagosome markers or ultrastructural
608 approaches will strengthen localization and interpretation. Second, the *in vitro* phagocytosis assay
609 uses pHrodo-conjugated yeast/zymosan-like particles, which can engage receptors such as TLR2
610 and dectin-1. Consequently, the observed age- and region-dependent differences may reflect
611 pathway-specific responsiveness rather than global phagocytic capacity. Testing alternative cargos
612 (e.g., apoptotic bodies) and defined opsonization states will be necessary to assess generality.
613 Third, although the CR2-Crry intervention is designed to inhibit C3 activation and deposition, we
614 did not directly measure complement activation or target engagement within the SVZ following
615 treatment. This limits causal inference about the extent and spatial specificity of complement
616 inhibition in the niche and makes it difficult to distinguish direct complement effects from
617 downstream or systemic consequences.

Additional caveats apply to generalizability and mechanistic resolution. Our work focuses on discrete ages (3 and 12 months for most experiments), which captures a midlife transition but does not resolve the temporal ordering of microglial activation, phagocytic engagement, and progenitor decline across aging; denser longitudinal sampling would better establish sequence and potential thresholds. The CR2-Crry intervention may not be microglia-specific and could act on other niche cells or peripheral immune pathways, complicating attribution of effects to microglia versus the broader SVZ environment. Moreover, increases in EdU+ counts provide a useful proliferative readout but do not by themselves resolve whether the rescued proliferation reflects altered cell-cycle dynamics, survival, lineage progression, or changes in the composition of proliferating populations; additional phenotyping of EdU+ cells would sharpen interpretation. Finally, the scRNA-seq reanalysis provides supportive mechanistic context, but transcriptomic signatures cannot distinguish increased phagocytic "capacity" from compensatory programs or assign directionality of cell–cell interactions; functional perturbations of candidate receptor–ligand axes and direct measures of engulfment dynamics will be required to establish causality.

638 # References

639 Ahlenius, H., Visan, V., Kokaia, M., Lindvall, O., & Kokaia, Z. (2009). Neural stem and
640 progenitor cells retain their potential for proliferation and differentiation into functional neurons
641 despite lower number in aged brain. *The Journal of Neuroscience*, *29*(14), 4408–4419.
642 https://doi.org/10.1523/JNEUROSCI.6003-08.2009

643 Alawieh, A., Zandian, J., & Feng, W. (2018). Factors affecting post-stroke motor recovery:
644 Implications on neurotherapy after brain injury. *Behavioural Brain Research*, *340*, 94–101.
645 https://doi.org/10.1016/j.bbr.2016.08.029

646 Alvarez-Buylla, A., & García-Verdugo, J. M. (2002). Neurogenesis in adult subventricular zone.
647 *The Journal of Neuroscience*, *22*(3), 629–634. https://doi.org/10.1523/JNEUROSCI.22-03-
648 00629.2002

649 Atkinson, C., Song, H., Lu, B., Qiao, F., Burns, T. A., Holers, V. M., Tsokos, G. C., &
650 Tomlinson, S. (2005). Targeted complement inhibition by C3d recognition ameliorates tissue
651 injury without apparent increase in susceptibility to infection. *Journal of Clinical Investigation*,
652 *115*(9), 2444–2453. https://doi.org/10.1172/JCI25208

653 Cunningham, C. L., Martínez-Cerdeño, V., & Noctor, S. C. (2013). Microglia regulate the
654 number of neural precursor cells in the developing cerebral cortex. *The Journal of Neuroscience*,
655 *33*(10), 4216–4233. https://doi.org/10.1523/JNEUROSCI.3441-12.2013

656 Cutler, R. R., & Kokovay, E. (2020). Rejuvenating subventricular zone neurogenesis in the aging
657 brain. *Current Opinion in Pharmacology*, *50*, 1–8. https://doi.org/10.1016/j.coph.2019.10.005

658 Deczkowska, A., Keren-Shaul, H., Weiner, A., Colonna, M., Schwartz, M., & Amit, I. (2018).
659 Disease-associated microglia: A universal immune sensor of neurodegeneration. *Cell*, *173*(5),
660 1073–1081. https://doi.org/10.1016/j.cell.2018.05.003

661 Doetsch, F., Caillé, I., Lim, D. A., García-Verdugo, J. M., & Alvarez-Buylla, A. (1999).
662 Subventricular zone astrocytes are neural stem cells in the adult mammalian brain. *Cell*, *97*(6),
663 703–716. https://doi.org/10.1016/s0092-8674(00)80783-7

664 Dulken, B. W., Buckley, M. T., Navarro Negredo, P., Saligrama, N., Cayrol, R., Leeman, D. S.,
665 ... & Brunet, A. (2019). Single-cell analysis reveals T cell infiltration in old neurogenic niches.
666 *Nature*, *571*(7764), 205–210. https://doi.org/10.1038/s41586-019-1362-5

667 Enwere, E., Shingo, T., Gregg, C., Fujikawa, H., Ohta, S., & Weiss, S. (2004). Aging results in
668 reduced epidermal growth factor receptor signaling, diminished olfactory neurogenesis, and
669 deficits in fine olfactory discrimination. *The Journal of Neuroscience*, *24*(38), 8354–8365.
670 https://doi.org/10.1523/JNEUROSCI.2751-04.2004

671 Ginhoux, F., Greter, M., Leyane, M., Nandi, S., See, P., Sivasankar, B., ... & Merad, M. (2010).
672 Fate mapping analysis reveals that adult microglia derive from primitive macrophages. *Science*,
673 *330*(6005), 841–845. https://doi.org/10.1126/science.1194637

674 Goings, D. E., Kozlowski, K. A., & Szele, F. G. (2006). Differential activation of microglia in
675 neurogenic versus non-neurogenic regions of the forebrain. *Glia*, *54*(4), 329–342.
676 https://doi.org/10.1002/glia.20381

677 Grabert, K., Michoel, T., Karavolos, M. H., Clohisey, S., Baillie, J. K., Stevens, M. P., ... &
678 McColl, B. W. (2016). Microglial brain region-dependent diversity and selective regional
679 sensitivities to aging. *Nature Neuroscience*, *19*(3), 504–516. https://doi.org/10.1038/nn.4222

680 Haney, M. S., Bohlen, C. J., Morgens, D. W., Ousey, J. A., Barkal, A. A., Tsui, C. K., ... &
681 Bassik, M. C. (2018). Identification of phagocytosis regulators using magnetic genome-wide
682 CRISPR screens. *Nature Genetics*, *50*(12), 1716–1727. https://doi.org/10.1038/s41588-018-
683 0254-1

684 Hu, B., Duan, S., Wang, Z., Li, X., Zhou, Y., Zhang, X., ... & Zheng, H. (2021). Insights into the
685 role of CSF1R in the central nervous system and neurological disorders. *Frontiers in Aging*
686 *Neuroscience*, *13*, 789834. https://doi.org/10.3389/fnagi.2021.789834

687 Izgi, H., Han, D., Isildak, U., Huang, S., Kocabiyik, E., Khaitovich, P., Somel, M., & Dönertaş,
688 H. M. (2022). Inter-tissue convergence of gene expression during ageing suggests age-related
689 loss of tissue and cellular identity. *eLife*, *11*, e68048. https://doi.org/10.7554/eLife.68048

690 Kalamakis, G., Brüne, D., Ravichandran, S., Bolz, J., Fan, W., Ziebell, F., ... & Martin-Villalba,
691 A. (2019). Quiescence modulates stem cell maintenance and regenerative capacity in the aging
692 brain. *Cell*, *176*(6), 1407–1419. https://doi.org/10.1016/j.cell.2019.01.040

693 Kapellos, T. S., Taylor, L., Lee, H., Cowley, S. A., James, W. S., Iqbal, A. J., & Greaves, D. R.
694 (2016). A novel real time imaging platform to quantify macrophage phagocytosis. *Biochemical*
695 *Pharmacology*, *116*, 107–119. https://doi.org/10.1016/j.bcp.2016.07.011

696 Khalaji, A., Yancheshmeh, F. B., Farham, F., Khorram, A., Sheshbolouki, S., Zokaei, M.,
697 Vatankhah, F., & Soleymani-Goloujeh, M. (2023). Don't eat me/eat me signals as a novel
698 strategy in cancer immunotherapy. *Heliyon*, *9*(10), e20507.
699 https://doi.org/10.1016/j.heliyon.2023.e20507

700 Kim, E. J., Ables, J. L., Dickel, L. K., Eisch, A. J., & Johnson, J. E. (2011). Ascl1 (Mash1)
701 defines cells with long-term neurogenic potential in subgranular and subventricular zones in
702 adult mouse brain. *PLoS One*, *6*(3), e18472. https://doi.org/10.1371/journal.pone.0018472

703 Li, W. (2012). Eat-me signals: Keys to molecular phagocyte biology and "appetite" control.
704 *Journal of Cellular Physiology*, *227*(4), 1291–1297. https://doi.org/10.1002/jcp.22815

705 Liang, H., Zhang, H., Geng, A., Mao, M., Tong, S., Tu, S., ... & Chen, S. T. (2019). Region-
706 specific and activity-dependent regulation of SVZ neurogenesis and recovery after stroke.
707 *Proceedings of the National Academy of Sciences*, *116*(27), 13621–13630.
708 https://doi.org/10.1073/pnas.1811825116

709 Liberzon, A., Birger, C., Thorvaldsdóttir, H., Ghandi, M., Mesirov, J. P., & Tamayo, P. (2015).
710 The Molecular Signatures Database (MSigDB) hallmark gene set collection. *Cell Systems*, *1*(6),
711 417–425. https://doi.org/10.1016/j.cels.2015.12.004

712 Lim, D. A., & Alvarez-Buylla, A. (2016). The adult ventricular–subventricular zone (V-SVZ)
713 and olfactory bulb (OB) neurogenesis. *Cold Spring Harbor Perspectives in Biology*, *8*(5),
714 a018820. https://doi.org/10.1101/cshperspect.a018820

715 Lledo, P. M., & Valley, M. T. (2016). Adult olfactory bulb neurogenesis. *Cold Spring Harbor*
716 *Perspectives in Biology*, *8*(8), a018945. https://doi.org/10.1101/cshperspect.a018945

717 Love, M. I., Huber, W., & Anders, S. (2014). Moderated estimation of fold change and
718 dispersion for RNA-seq data with DESeq2. *Genome Biology*, *15*(12), 550.
719 https://doi.org/10.1186/s13059-014-0550-8

720 Luo, J., Daniels, S. B., Lennington, J. B., Notti, R. Q., & Conover, J. C. (2006). The aging
721 neurogenic subventricular zone. *Aging Cell*, *5*(2), 139–152. https://doi.org/10.1111/j.1474-
722 9726.2006.00197.x

723 Marshall, G. P., Deleyrolle, L. P., Reynolds, B. A., Steindler, D. A., & Laywell, E. D. (2014).
724 Microglia from neurogenic and non-neurogenic regions display differential proliferative
725 potential and neuroblast support. *Frontiers in Cellular Neuroscience*, *8*, 180.
726 https://doi.org/10.3389/fncel.2014.00180

727 Maslov, A. Y., Barone, T. A., Plunkett, R. J., & Pruitt, S. C. (2004). Neural stem cell detection,
728 characterization, and age-related changes in the subventricular zone of mice. *The Journal of*
729 *Neuroscience*, *24*(7), 1726–1733. https://doi.org/10.1523/JNEUROSCI.4608-03.2004

730 Morrison, V., Holloway, M. G., Taylor, J. B., Bassik, A. A., Kim, P. J., Kim, K. A., ... & Carter,
731 B. D. (2023). Jedi-1/MEGF12-mediated phagocytosis controls the pro-neurogenic properties of
732 microglia in the ventricular-subventricular zone. *bioRxiv*.
733 https://doi.org/10.1101/2023.03.03.531012

734 Nath, S., Martínez Santamaría, J. C., Chu, Y. H., Choi, J. S., Conforti, P., Lin, J. D., ... &
735 Schachtrup, C. (2024). Interaction between subventricular zone microglia and neural stem cells
736 impacts the neurogenic response in a mouse model of cortical ischemic stroke. *Nature*
737 *Communications*, *15*(1), 9095. https://doi.org/10.1038/s41467-024-53217-1

738 Ohab, J. J., Fleming, S., Blesch, A., & Carmichael, S. T. (2006). A neurovascular niche for
739 neurogenesis after stroke. *The Journal of Neuroscience*, *26*(50), 13007–13016.
740 https://doi.org/10.1523/JNEUROSCI.4323-06.2006

741 Pluvinage, J. V., Haney, M. S., Smith, B. A. H., Sun, J., Iram, T., Bonanno, L., ... & Wyss-
742 Coray, T. (2019). CD22 blockade restores homeostatic microglial phagocytosis in ageing brains.
743 *Nature*, *568*(7751), 187–192. https://doi.org/10.1038/s41586-019-1088-4

744 Robin, A. M., Zhang, Z. G., Wang, L., Zhang, R. L., Katakowski, M., Zhang, L., ... & Chopp, M.
745 (2006). Stromal cell-derived factor 1alpha mediates neural progenitor cell motility after focal
746 cerebral ischemia. *Journal of Cerebral Blood Flow & Metabolism*, *26*(1), 125–134.
747 https://doi.org/10.1038/sj.jcbfm.9600172

748 Shigemoto-Mogami, Y., Hoshikawa, K., Goldman, J. E., Sekino, Y., & Sato, K. (2014).
749 Microglia enhance neurogenesis and oligodendrogenesis in the early postnatal subventricular
750 zone. *The Journal of Neuroscience*, *34*(6), 2231–2243.
751 https://doi.org/10.1523/JNEUROSCI.1619-13.2014

752 Solano, F. G., Ma, S., Ameloot, D. M., Rivera, R., D'Amours, A., Chemtob, S., ... & Kokovay,
753 E. (2016). Neurogenic niche microglia undergo positional remodeling and progressive activation
754 contributing to age-associated reductions in neurogenesis. *Stem Cells and Development*, *25*(7),
755 542–555. https://doi.org/10.1089/scd.2015.0319

756 Song, H., He, C., Knaak, C., Guthridge, J. M., Holers, V. M., & Tomlinson, S. (2003).
757 Complement receptor 2–mediated targeting of complement inhibitors to sites of complement
758 activation. *Journal of Clinical Investigation*, *111*(12), 1875–1885.
759 https://doi.org/10.1172/JCI17348

760 Tan, Y., Zheng, Y., & Tang, L. (2020). Microglial regional heterogeneity and its role in the
761 brain. *Molecular Psychiatry*, *25*(2), 351–367. https://doi.org/10.1038/s41380-019-0609-8

762 Xavier, A. L., Kress, B. T., Goldman, S. A., de Menezes, J. R., & Nedergaard, M. (2015). A
763 distinct population of microglia supports adult neurogenesis in the subventricular zone. *The*
764 *Journal of Neuroscience*, *35*(34), 11848–11861. https://doi.org/10.1523/JNEUROSCI.1217-
765 15.2015

766 Yamashita, T., Ninomiya, M., Hernández Acosta, P., García-Verdugo, J. M., Sunabori, T.,
767 Sakaguchi, M., ... & Sawamoto, K. (2006). Subventricular zone-derived neuroblasts migrate and
768 differentiate into mature neurons in the post-stroke adult striatum. *The Journal of Neuroscience*,
769 *26*(24), 6541–6552. https://doi.org/10.1523/JNEUROSCI.0149-06.2006

770 Yen, J. H., & Yu, I. C. (2024). The role of ApoE-mediated microglial lipid metabolism in brain
771 aging and disease. *Immunometabolism*, *5*(1), e00018.
772 https://doi.org/10.1097/IN9.0000000000000018

773 Yu, G., Wang, L. G., Han, Y., & He, Q. Y. (2012). clusterProfiler: An R package for comparing
774 biological themes among gene clusters. *OMICS: A Journal of Integrative Biology*, *16*(5), 284–
775 287. https://doi.org/10.1089/omi.2011.0118

776